Implementation of Non-Reflecting Boundary Conditions in a Finite Volume Unstructured Solver for the Study of Turbine Cascades

IMPLEMENTATION OF NON-REFLECTING BOUNDARY CONDITIONS IN A FINITE VOLUME UNSTRUCTURED SOLVER FOR THE STUDY OF TURBINE CASCADES

Giove De Cosmo[a,*], *Simone Salvadori*[b,†]

[a]Polytechnic of Turin, Turin, Italy
[b]Department of Industrial Engineering, University of Florence, Florence, Italy

ABSTRACT

The analysis of component interaction in the turbomachinery field is nowadays of growing importance. This leads to the combination of different approaches, such as Large Eddy Simulation for combustors and Unsteady Reynolds-Averaged Navier-Stokes equations for turbines, and is responsible for the increase of both computational effort and required accuracy of the numerical tools. To guarantee accurate results and efficient convergence rates, numerical schemes must handle the spurious reflecting waves coming from the boundaries of truncated domains. This can be achieved by means of Non-Reflecting Boundary Conditions. The research activity described in the present paper is aimed at implementing the method of Non-Reflecting Boundary Conditions for the Linearized Euler Equations proposed by Giles in an in-house finite volume implicit time-marching solver. The methodology is validated using the available experimental data obtained at the von Karman Institute for Fluid Dynamics on the LS89 High-Pressure Turbine vane for both subsonic and transonic working conditions. The implemented approach demonstrates its importance for the correct evaluation of the pressure distribution both on the vane surface and in the pitchwise direction when the computational domain is truncated at the experimental probe's position.

KEYWORDS

Non-Reflecting Boundary Conditions, Implicit Solver, Computational Fluid Dynamics, LS89, High-Pressure Vane

NOMENCLATURE

Latin

$\mathbf{A}, \mathbf{B}$	Coefficient matrix of the hyperbolic system of PDE in the x, y-direction
a_n	Weight coefficient of the Fourier decomposition in the x-direction
C, C_{ax}	Blade chord/axial chord
c_i	Characteristic quantity component
$\tilde{c}_i, \bar{c}_i$	Local/Average value of the i-th characteristic
$\hat{c}_{i,l}$	l-th harmonic of the i-th characteristic
E	Total energy
F_i	i-th component of the convective flux
$\bar{F}_i$	i-th component of the averaged convective flux
$\mathbf{I}$	Identity matrix

*Currently at the von Karman Institute for Fluid Dynamics, Rhode-Saint-Genèse, Belgium
†Contact author: simone.salvadori@unifi.it

i	Imaginary unit
j	Boundary cell index
k	x-direction eigenvalue
l	y-direction eigenvalue
M_{is}	Isentropic Mach number
N	Total number of outlet boundary cells
P	Cascade pitch
p	Pressure
p_0	Inlet total pressure
p_{out}	Outlet user-defined pressure
$\mathbf{s}$	2D steady limit of the auxiliary eigenvector
T_0	Inlet total temperature
$\mathbf{U}$	Vector of thermodynamic properties
$\hat{\mathbf{U}}_l$	l^{th} harmonic of $\mathbf{U}$ along the y-direction
$\mathbf{u}$	Main eigenvector of the sample EVP
u, v, w	x, y, z-direction velocity
$\mathbf{v}$	Auxiliary eigenvector

Greek

β	Complex coefficient
γ	Specific heat ratio
δ	Perturbation
ω	t-eigenvalue
ρ	Density

INTRODUCTION

Modern algorithms for the numerical solution of the Navier-Stokes equations are often based on high-order schemes, whose potential is critically reliant on the correct implementation of the boundary conditions. This is especially true when the equations have to be solved on a truncated finite domain. In fact, the hyperbolic nature of the Navier-Stokes equations is associated with the presence of waves and, in the specific case of a cropped domain, some of them are propagating outward and some other inward. A set of boundary conditions that correctly describes the incoming waves is thus required to avoid spurious oscillations of the solution. These oscillations are quite annoying, since they can lead to considerable distortions of the flow pattern or even inhibit convergence to steady state.

The most common approach to derive such boundary conditions consists in suppressing all the incoming waves. This ideally prevents any non-physical reflection of the outgoing waves on the boundary. An important requirement on any numerical boundary condition is that it should lead to a well-posed problem. Therefore, these conditions must not damage the mathematical structure of the numerical problem.

Non-reflecting boundary conditions are critical in the calculation of turbomachinery flows. As observed by Giles (1990), the far-field boundary in turbomachinery simulations is typically no more than one chord away from the blade. Consequently, the far-field contains a significant component of several different spatial wavenumbers. These waves have to be adequately controlled and eventually suppressed, in order to get a consistent physical solution that is independent of the location of the boundary.

The goal of this research is to implement non-reflecting boundary conditions in a finite vol-

ume solver and to verify the effects of this treatment on the performance of the code. The solver chosen for the present activity is *HybFlow*, a finite volume, implicit solver for the Navier-Stokes equations on unstructured meshes. The reference theory for this implementation has been in development since the early 1970s and consists of several different methods. In this context the approach developed by Giles (1990) is considered. It is called Non-Reflecting Boundary Conditions for the Linearized Euler Equations, here referred to as NRBC-LEE.

The implementation of the NRBC-LEE method is validated on the LS89 airfoil, a well-known test case from literature (see Arts et al. (1990)). Two working conditions (subsonic and transonic) are selected and the pressure distribution deriving from the application of the NRBC-LEE method is compared to the baseline, reflecting one.

NON-REFLECTING BOUNDARY CONDITIONS

Numerical treatments to avoid wave reflection on the boundary of truncated domains are known in literature by different names: radiation, transparent, open, non-reflecting, artificial (boundary conditions). The denomination of Artificial Boundary Conditions (ABCs) is representative of the fact that these conditions are introduced only to provide the numerical simulation with the information lost with the domain truncation.

As observed by Givoli & Neta (2003) it is difficult to find a single ABC that is general, easy to implement in a numerical scheme and able to keep it stable, accurate and efficient. Therefore, a lot of theories exist, each of them optimised for a few, specific, applications. The minimal requirement for any ABC is to ensure solvability of the truncated problem, but the chosen set of boundary conditions must also guarantee that the artificial problem solution is as close as possible to the solution of the original unbounded problem. In case of exact coincidence between the two solutions, an *exact* ABC has been formulated.

According to Tsynkov (1998), artificial boundary conditions can be classified in three main categories: global methods, local methods and absorbing layers.

Global methods One of the first theories to be published on the topic of absorbing boundary conditions for stationary problems is that of Engquist & Majda (1977). The authors perform the decomposition of the solution as a superimposition of waves. Then, they eliminate all the incoming waves at the far-field boundary, making it non-reflecting. The implementation of exact ABCs for time-dependent problems is generally difficult, due to the additional non-locality in time of the boundary conditions. Givoli & Cohen (1995) introduce two nested artificial boundaries. They perform a time advance on the solution at the exterior boundary, using the available values at the previous time steps on the interior boundary. Global methods are accurate and robust, but complex and computationally expensive.

Local methods Local ABCs are preferred because they substantially simplify the numerical algorithm. In turn, the localisation process reduces the numerical accuracy of the original exact ABC. Higher-order conditions provide better accuracy than lower-order ones, whereas low-order approximations have fewer geometric limitations. The classical approach to calculate local ABCs consists in developing rational approximations to the non-local operators, getting differential (i.e. local) conditions. Usually, Taylor or Padè approximations are used, see Engquist & Majda (1977). Some authors, like Gustafsson (1988), develop different rational approximations in space and time. A different approach to approximate the exact ABCs

consists of selecting only a few leading terms in the far-field asymptotic expansion of the solution and then using this truncated expansion to set the ABCs. Bayliss & Turkel (1982) give a contribution to this method.

Some techniques are based on the analysis of characteristics. They turn out to be simple, cheap, universal and suitable for both steady and unsteady problems. Moreover, they do not require the previous construction of an exact ABC. Hedstrom (1979) works on the method of characteristics for the one-dimensional Euler system. Thompson (1990) extends the characteristic radiation boundary conditions to multidimensional problems. However, this approach remains essentially one-dimensional at each boundary point. Therefore, the boundary cannot be expected to behave in a fully transparent way for general-direction outgoing waves.

The analysis of boundary conditions for viscous flows concerns the incompletely parabolic PDEs, studied by Halpern (1991). The treatment of artificial, viscous boundaries can be performed in the same way as for Euler equations. In this case, however, it is essential to carry out a well-posedness analysis, as done by Rudy & Strikwerda (1981). Poinsot & Lele (1992) specifically derive Local One-Dimensional Inviscid Navier-Stokes Characteristic Boundary Conditions (LODI-NSCBC) for application to direct numerical simulation.

Absorbing layers Absorbing layers were primarily developed in the Computational Electro-Magnetics (CEM) and they are also referred to as *sponge layers*, *exit zones* or *buffer zones*. As pointed out by Hu (2007), this strategy consists in introducing additional zones of grid points around the physical domain that are able to significantly attenuate the outgoing disturbances. The boundary between the computational domain and the layer should also cause minimal reflections: see the Perfectly Matched Layer (PML) theory developed by Berenger (1994). The first applications of the PML technique to the Euler equations are ascribed to Hu (1996) and Abarbanel & Gottlieb (1997).

THE NRBC-LEE THEORY

The NRBC-LEE theory is mainly summarised in three papers: Giles (1988), Giles (1990) and Giles (1991). The proposed numerical treatment avoids wave reflections at the domain boundaries, resulting in a correct reproduction of the pitchwise pressure distribution along the boundary itself. This outcome allows for the shortening of the computational domain of blade cascade simulations, with a significant increase in the calculations efficiency. The NRBC-LEE theory is formulated both for inlet and outlet boundaries, in steady and unsteady conditions. In this paper only the treatment of steady, outlet boundaries is considered.

Giles' theory is explicitly suited for unsteady linear systems. This implies the principle of superimposition to be valid and the solution can hence be decomposed into a sum of modes to be analysed separately. Therefore, exact non-reflecting boundary conditions can be constructed. The NRBC-LEE method can be extended to some non-linear systems in which the amplitude of perturbations is sufficiently small. This is usually the case of the far-field.

2D steady NRBC-LEE method Giles develops its method for an unsteady, two-dimensional, hyperbolic system of partial differential equations. It can be associated to an EigenValue Problem (EVP) in x, y and t, with eigenvalues k, l and ω, respectively

$$\frac{\partial \mathbf{U}}{\partial t} + \mathbf{A}\frac{\partial \mathbf{U}}{\partial x} + \mathbf{B}\frac{\partial \mathbf{U}}{\partial y} = 0 \quad \Rightarrow \quad (-\omega \mathbf{I} + k\mathbf{A} + l\mathbf{B})\mathbf{u} = 0 \tag{1}$$

The solution of this EVP leads to a set of right and left eigenvectors ($\mathbf{u}^R$ and $\mathbf{u}^L$). Moreover, a set of auxiliary left eigenvectors can be identified, defined as $\mathbf{v}^L = \mathbf{A}^{-1}\mathbf{u}^L$.

Suppose that the differential equation has to be solved in the domain $x > 0$ and that non-reflecting conditions have to be derived at the boundary $x = 0$. At each boundary point, the solution $\mathbf{U}$ can be decomposed in a sum of N, x-direction Fourier modes

$$\mathbf{U}(x, y, t) = \left[\sum_{n=1}^{N} a_n \mathbf{u}_n^R e^{ik_n x} \right] e^{i(ly - \omega t)} \tag{2}$$

being k_n the n^{th} eigenvalue in the x direction, at fixed values of ω and l ($l/\omega = \lambda$). Therefore, the ideal non-reflecting boundary condition requires that $a_n = 0$ for each n corresponding to an incoming wave. This is equivalent to impose $\mathbf{v}_n^L \mathbf{U} = 0$ for each incoming x-direction wavenumber k_n. The latter is the *non-local* ABC.

The most relevant local approximation of the exact ABC is the 2D, steady, single-frequency boundary condition. It can be obtained in the limit $\omega \to 0$ ($\lambda \to \infty$) for each incoming wave n and y-direction Fourier mode l

$$\mathbf{s}_n^L = \lim_{\lambda \to \infty} \mathbf{v}_n^L(\lambda) \quad \Rightarrow \quad \mathbf{s}_n^L \hat{\mathbf{U}}_l = 0 \tag{3}$$

where $\mathbf{s}_n^L$ is the steady auxiliary left eigenvector and $\hat{\mathbf{U}}_l$ the l-th harmonic of U in the y-direction. The boundary condition for the $l = 0$ mode is $\mathbf{v}_n^L(0)\hat{\mathbf{U}}_0 = 0$ and it is associated to an indeterminate form. This represents the solution average at the boundary and it can be modified by the user to specify the value of the average incoming characteristics.

Quasi-3D NRBC-LEE method The NRBC-LEE theory developed by Giles is specifically addressed to 2D cases. However, in Saxer & Giles (1993) the 2D approach is extended to 3D turbomachinery problems, leading to the quasi-3D NRBC-LEE method. According to the authors, the tangential direction can be decoupled from the radial one. The former can be treated in terms of the 2D exact NRBC-LEE method, while the latter only introduces discrete stations where the 2D procedure has to be repeated. Then, the core of the quasi-3D NRBC-LEE method remains 2D. Therefore, even though the full theory is presented in the following, a 2D test case is chosen to validate the implementation.

THE HYBFLOW SOLVER

Hybflow is a finite-volume CFD solver, written in FORTRAN (F90). It is aimed at simulating turbomachinery flows by solving the compressible Navier-Stokes equations in conservative form on unstructured grids. The solver works with 3D domains, then 2D domains are properly extruded to make them three-dimensional. *HybFlow* is a non-dimensional code, meaning that all the quantities involved in the calculation are related to some reference value. This choice is useful to enlighten the order of magnitude of the phenomena involved in the simulation.

HybFlow uses the MUSCL numerical scheme for the spatial discretization. Two gradient reconstruction methods are implemented in the code, a linear Finite Volume (FVM) reconstruction and a Least SQuare (LSQ) reconstruction. The first one evaluates the face mean value of the solution by considering the elements adjacent to the present cell and calculating a distance-weighted average. The second one, as suggested by Anderson & Bonhaus (1994), considers

the elements adjacent to the neighbouring cell, too. These two alternatives are both 2nd order-accurate. Slope limiters are needed in order to guarantee the monotonicity of the solution even in presence of highly non-linear phenomena, like shocks.

The stationary solution of the Navier-Stokes equations in *HybFlow* is calculated through an implicit, time-marching method. An iterative Newton method is used to solve the non-linear system. The Generalized Mean RESidual (GMRES) approach is implemented for the matrix inversion. Since Newton methods are unstable for highly variable solutions and they converge slowly, an Incomplete LU (ILU) preconditioning is introduced, in order to save both computational time and memory (see Saad & Schultz (1986)). A dual time-stepping approach is implemented for time-dependent problems. Turbulence is modelled using the traditional two equation $\kappa - \omega$ model by Wilcox (1993).

HybFlow makes use of a multi-block procedure to save CPU and memory. This methodology subdivides the computational grid in blocks of cells, in order to reduce the rank of the matrix to be inverted. The multi-block strategy is also required for parallel computing. This allows a consistent speedup, even proportional to the number of processors. Usually the number of blocks is much higher than the number of processors and hence each processor handles several blocks. The solver parallelisation is based on the Message-Passage Interface (MPI) standard.

HybFlow has been extensively validated for the aero-thermal analysis of turbomachinery flows as showed by Montis et al. (2014), Carnevale et al. (2013), Salvadori et al. (2013), Salvadori et al. (2011), and Montomoli et al. (2011).

IMPLEMENTATION OF THE NRBC-LEE APPROACH

Giles (1991) presents a detailed description of the implementation of his theory in an explicit solver based on the Lax-Wendroff algorithm. In this research the NRBC-LEE theory is adapted to an implicit solver. This is possible since the NRBC-LEE method just modifies the boundary values of the solution, without affecting the solver core functioning.

Flow state linearization The flow average state on the outlet boundary must be calculated. Giles (1991) proposes a 2D flux-averaged procedure, here completed by adding the 3rd dimension contribution. First, the convective fluxes on each boundary face are computed from the set of primitive variables (ρ, u, v, w, p)

$$F_1 = \rho u \qquad F_2 = \rho u^2 + p \qquad F_3 = \rho uv \qquad F_4 = \rho uw \qquad F_5 = u(\rho E + p) \tag{4}$$

recalling that the total energy E can be expressed in terms of the same primitive variables

$$E = \frac{p}{\gamma - 1} + \frac{1}{2}\rho(u^2 + v^2 + w^2) \tag{5}$$

Each flux component F_i can be averaged on the outlet boundary simply calculating its arithmetic mean $\bar{F}_i$ over the border cells

$$\bar{F}_i = \frac{1}{N}\sum_{j=1}^{N} F_{i,j} \tag{6}$$

where N is the overall number of outlet cells and j is the local cell index ($j \in [1; N]$). The expressions in Equation 4 can be solved for the primitive variables as a function of the averaged

fluxes, leading to the flux-averaged primitive quantities $(\rho_F, u_F, v_F, w_F, p_F)$

$$
\begin{aligned}
p_F &= \frac{1}{\gamma+1}\left(\bar{F}_2 + \sqrt{\bar{F}_2^2 + (\gamma^2-1)(\bar{F}_2^2 + \bar{F}_3^2 + \bar{F}_4^2 - 2\bar{F}_1\bar{F}_5)}\right) \\
u_F &= \frac{\bar{F}_2 - p_F}{\bar{F}_1} \quad v_F = \frac{\bar{F}_3}{\bar{F}_1} \qquad w_F = \frac{\bar{F}_4}{\bar{F}_1} \qquad \rho_F = \frac{\bar{F}_1}{u_F}
\end{aligned}
\tag{7}
$$

These equations have to be transformed as to make them compatible with *HybFlow* non-dimensional variables.

Other kinds of averaging procedures can be encountered in literature. De Raedt (2015) proposes an area averaging of the fluxes or even a simple area averaging of the flow properties for those cases in which $u \approx 0$. However, once the average flow properties are known, the linearization can be performed and the perturbation (δ) quantities can be obtained. Giles uses the nodal changes calculated by the Lax-Wendroff algorithm as perturbation variables. In this procedure, instead, the perturbations on each cell j are calculated by means of flow linearization around the flux-averaged properties:

$$
\begin{pmatrix} \delta\rho \\ \delta u \\ \delta v \\ \delta w \\ \delta p \end{pmatrix}_j = \begin{pmatrix} \rho - \rho_F \\ u - u_F \\ v - v_F \\ w - w_F \\ p - p_F \end{pmatrix}_j
\tag{8}
$$

DFT in the characteristic space Once the perturbation (δ) variables are known, the local characteristic variables c_i are calculated on each boundary cell j. Notice that the transformation matrix is constant and it contains just the flux-averaged quantities

$$
\begin{pmatrix} c_1 \\ c_2 \\ c_3 \\ c_4 \\ c_5 \end{pmatrix}_j = \begin{pmatrix} -c_F^2 & 0 & 0 & 0 & 1 \\ 0 & 0 & \rho_F c_F & 0 & 0 \\ 0 & 0 & 0 & \rho_F c_F & 0 \\ 0 & \rho_F c_F & 0 & 0 & 1 \\ 0 & -\rho_F c_F & 0 & 0 & 1 \end{pmatrix} \begin{pmatrix} \delta\rho \\ \delta u \\ \delta v \\ \delta w \\ \delta p \end{pmatrix}_j
\tag{9}
$$

Then, the Discrete Fourier Transform (DFT) is calculated for the 2[nd] and the 4[th] characteristic variables ($\hat{c}_{2l}$ and $\hat{c}_{4l}$)

$$
\hat{c}_{2l} = \sum_{j=1}^{N} c_{2j} e^{-i2\pi \frac{j}{N} l} \qquad \hat{c}_{4l} = \sum_{j=1}^{N} c_{4j} e^{-i2\pi \frac{j}{N} l}
\tag{10}
$$

where l is the harmonic number. In particular, due to the relation between positive and negative harmonics (complex conjugate pairs), just half $(N/2 - 1)$ of the complex Fourier coefficients are needed. These coefficients are global, not depending on the cell index.

The ratio j/N identifies the non-dimensional position of the j-th cell along the outlet boundary, as it is required to calculate the DFT. Unless the outlet mesh is perfectly regular, it would be more rigorous to calculate the non-dimensional position in terms of the effective geometrical coordinate of the cell. Nevertheless, this solution seems to make the calculation unstable and it is discarded. The error introduced is smaller as the number of outlet cells increases.

However, in order to define the right value for the j/N coefficient, the boundary cells must be in the correct order. If this is not guaranteed, they must be sorted according to their position along the boundary. Therefore, a sorting cycle is performed in any case at the beginning of the procedure, as suggested by De Raedt (2015).

Calculation of the incoming characteristic At a subsonic outflow the first four characteristics are outgoing and only the 5th characteristic variable needs to be calculated. The incoming characteristic ($\hat{c}_{5l}$) must be derived from the outgoing ones ($\hat{c}_{2l}$ and $\hat{c}_{4l}$) per each harmonic l, as indicated by Saxer & Giles (1993)

$$\hat{c}_{5l} = \frac{2u_F}{\beta - v_F}\hat{c}_{2l} - \frac{\beta + v_F}{\beta - v_F}\hat{c}_{4l} \tag{11}$$

where the coefficient β is defined as

$$\beta = \begin{cases} i\,\text{sign}(l)\sqrt{1 - u_F^2 - v_F^2} & \text{if} \quad u_F^2 + v_F^2 < 1 \\ -\text{sign}(v_F)\sqrt{u_F^2 + v_F^2 - 1} & \text{if} \quad u_F^2 + v_F^2 > 1 \end{cases} \tag{12}$$

The coefficients in Equation 11 depend only on the local value of the velocity and (eventually) on the harmonic number. However, with the previous choice for the range of harmonics, sign(l) is always positive. Notice that β is imaginary for subsonic flow and real for supersonic flow, reflecting the different behaviour of a perturbation propagating in these two flow regimes. It follows that the expression for $\hat{c}_{5l}$ is, in general, complex and it can be handled by separating the real and the imaginary parts.

This result is still non-local because it lays in the frequency space. Then, the single-sided Inverse DFT (IDFT) is performed to get the updated local amplitude of the 5th characteristic

$$\tilde{c}_{5j} = 2Re\left\{\sum_{l=1}^{N/2-1} \hat{c}_{5l} e^{i2\pi\frac{j}{N}l}\right\} \tag{13}$$

where the sum is multiplied by 2, in order to recover the information neglected with the reduction of the number of harmonics to $(N/2 - 1)$. The ideal local value of the 5th characteristic $\tilde{c}_{5j}$ must be corrected by means of the average value $\bar{c}_{5j}$ associated with the user-specified exit pressure p_{out}. A factor 2 is introduced, deriving from the observation that $\partial p/\partial c_5 = 1/2$

$$\bar{c}_{5j} = -2(p_F - p_{out}) \tag{14}$$

Finally, the local value for the 5th characteristic is

$$c_{5j} = \tilde{c}_{5j} - \bar{c}_{5j} \tag{15}$$

From characteristic to physical space The updated set of characteristic variables is used to get back to the physical space, by inverting the coefficient matrix in Equation 9. The new values obtained for the physical properties are then substituted to the original values.

	$\mathbf{p_0}$ [bar]	$\mathbf{T_0}$ [K]	$\mathbf{M}_{is}$	$\mathbf{p}$ [bar]
MUR43	1.435	$\approx$ 420	0.840	0.9040
MUR47	1.596	$\approx$ 420	1.020	0.8236

(a) **Flow conditions**

	LONG	**PROBE**
$\mathbf{d/c_{ax}}$	1.05	0.433
Elem	81k	74k

(b) **Domain characteristics**

Table 1: **Characteristics of the LS89 blade simulations**

Programming details The previously described operations take place at the end of each iteration. The computed solution is substantially *corrected* using the new boundary conditions to avoid spurious reflections.

Since *HybFlow* works on block-decomposed domains, the outlet faces could be split in more than one block. This is particularly frequent in case of refined grids. In the proposed implementation, the association of the outlet faces to more than one block does not affect the routine execution. In fact, the proper indexing vectors allows for direct access to each outlet face and make it possible to correctly perform the necessary operations also in a parallel environment.

Being the modification of the pitchwise boundary pressure profile the most evident effect of NRBC-LEE, the pre-existing boundary values (namely, the physical boundary condition) must be overwritten with the newly calculated values. This is particularly important if the physical boundary condition consists in a constant pressure profile.

VALIDATION

The NRBC-LEE method is validated on the LS89 test case, a 2D High-Pressure Turbine vane designed and tested at the von Karman Institute for Fluid Dynamics (see Arts et al. (1990)). The LS89 airfoil is still a popular case in the turbine field, as testified by a recent publication by Cação Ferreira et al. (2019), and is used for the validation of high-fidelity approaches in Computational Fluid Dynamics (CFD) (as in the recent work by Seguí et al. (2018)). Among the available experimental configurations, two are selected to be numerically tested with NRBC-LEE and then compared with the experiments (see Table 1a). Notice that the MUR43 layout is subsonic, while the MUR47 configuration is transonic. The Reynolds number for both the cases is 10^6.

Spatial discretization The tests are carried out on a LONG and a PROBE domain. The LONG domain is the baseline, while the PROBE domain is such that the outlet section is placed in correspondence of the downstream wall static pressure tappings. The domain and mesh characteristics are reported in Table 1b, where d is the distance trailing edge-outlet boundary and $Elem$ the total number of mesh elements.

All the grids are generated using the mesh generator CENTAUR™. As prescribed by best practices, each mesh is significantly refined near the blade wall to correctly resolve the boundary layer ($y^+ < 1$). The remaining part of the domain is discretised in a coarser way to limit the overall number of elements. An inlet sponge layer is introduced to damp reflections on the inlet boundary. A grid dependence analysis performed doubling the elements number for three meshes shows that the difference between the loss coefficient values calculated for the selected grid and the one evaluated for the finer one is lower than 0.05%. See Figure 1 for some visual details of the chosen mesh.

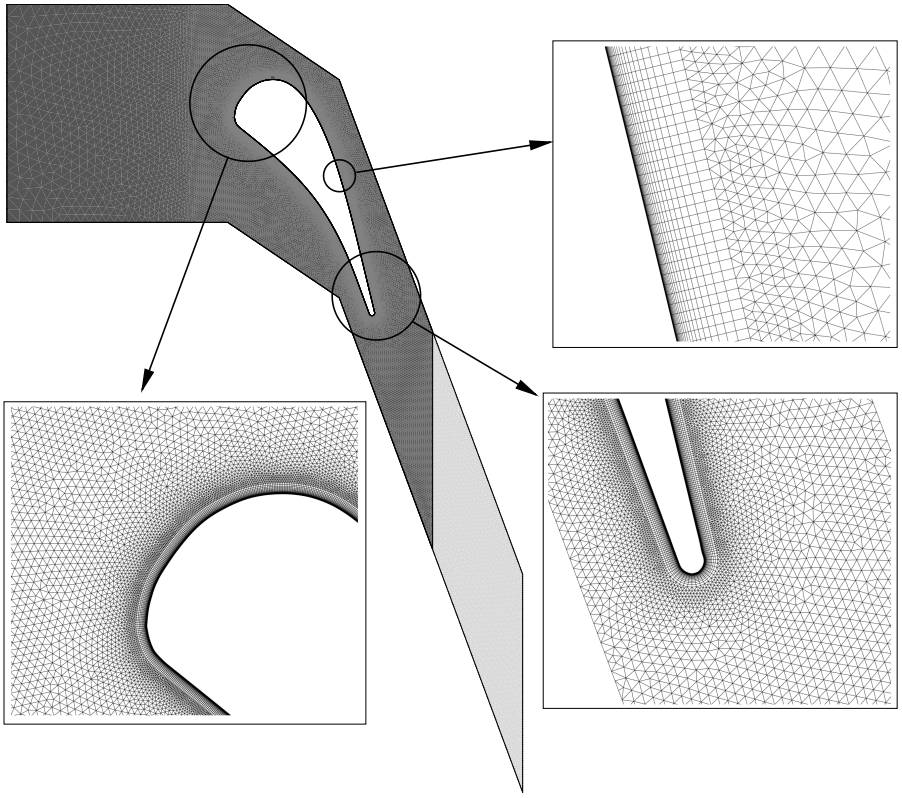

Figure 1: **Comparison between LS89 LONG and PROBE domains and mesh details**

	LONG	**PROBE**	**PROBE-NRBC**	**PROBE-EXP**
MUR43	3LQR	3PQR	3PQN	3PQE
MUR47	7LQR	7PQR	7PQN	7PQE

Table 2: **Test matrix for the LS89 blade simulations**

Test matrix The LONG domain is run with a classical constant-pressure outlet boundary condition. The PROBE domain is run considering either a constant-pressure outlet value or a non-reflecting boundary condition with a prescribed averaged pressure value or a pitchwise non-uniform pressure distribution. In the latter case, the experimental values are imposed. The test matrix is reported in Table 2.

All the calculations are carried out with the LSQ gradient reconstruction method, they are adiabatic and fully turbulent. The activation of the NRBC-LEE method prevents the calculations to reach residuals values below 10^{-5}, thus demonstrating that this treatment is non-conservative. However, all the calculations converge with a mass-flow error around 0.1%. Calculations are considered converged once the residuals values, the mass-flow error and the loss coefficient remain constant over 500 iterations or more.

Results: MUR43 Figure 2 compares the static pressure fields of 3LQR, 3PQR and 3PQN. All the solutions are very similar near the blade leading edge. Moving along the blade, the 3PQR solution gradually moves away from the 3LQR solution. This is due to the effect of

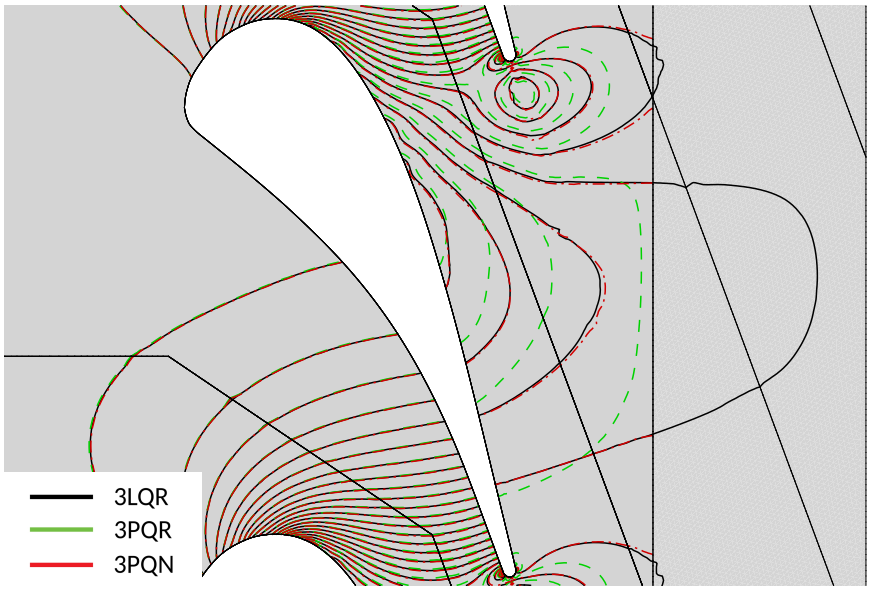

Figure 2: **MUR43 pressure fields comparison**

the constant-pressure boundary, that finally causes the iso-pressure lines to close right before the PROBE outlet. Notice that both the pressure distribution near the trailing edge and the one along the suction side are significantly affected by the reflecting behaviour of the outlet boundary. The 3LQR and 3PQN distributions, instead, are almost superimposed, except for some small differences near the PROBE outlet boundary. The iso-pressure lines are open at the outlet boundary both for 3LQR and 3PQN.

The pitchwise isentropic Mach number profiles of 3LQR, 3PQR, 3PQN and 3PQE at the PROBE outlet section are compared in Figure 3. The available experimental data are also included. The reason why only half of the 3PQE distribution reproduces the experimental data is that the numerical domain is periodic and only the portion of experimental data between $Y/P = 0.0$ and $Y/P = 1.0$ has been used as boundary condition. The 3PQR isentropic Mach number distribution is significantly different from the other cases. In fact the constant-pressure outlet boundary condition keeps the pressure almost uniform along the pitch. The 3PQN trend is essentially superimposed to the 3LQR trend (except near the maxima/minima, where less than 0.6% difference appears), but a lower average value of the isentropic Mach number is numerically predicted with respect to the experiments. Nevertheless, the experimental pressure distribution is correctly reproduced in terms of shape and variation. The 3PQE profile is, as expected, almost superimposed to the experimental points.

The numerical and experimental isentropic Mach number distributions on the blade surface are compared in Figure 4. The 3LQR and the 3PQN trends are almost superimposed and their difference with respect to the 3PQR distribution is of the order of 1.0%. However, some peculiarities arise on the rear suction side. Between $x/C_{ax} = 0.4$ and $x/C_{ax} = 0.75$ the 3PQR distribution seems to perform better than the 3PQN one, while in the remaining part of the suction side both 3LQR and 3PQN seem to better fit the experimental data. Apart from 3PQE, all the numerical results lead to a small underestimation of the blade loading with respect to the experiments. The 3PQE profile, instead, matches much better the experimental load. The latter result further underlines the importance of a correct definition of boundary conditions in CFD.

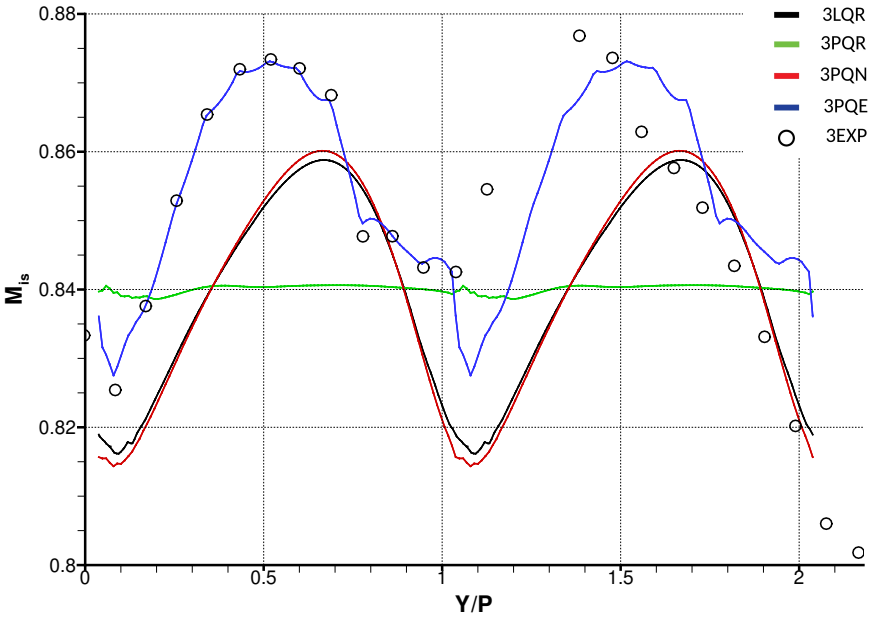

Figure 3: **MUR43 outlet isentropic Mach number distributions**

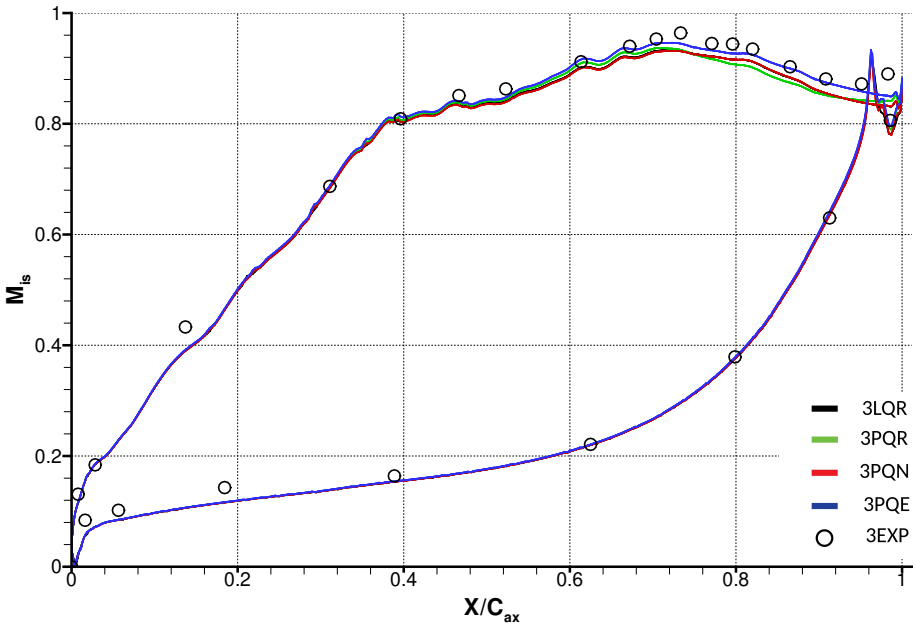

Figure 4: **MUR43 blade isentropic Mach number distributions**

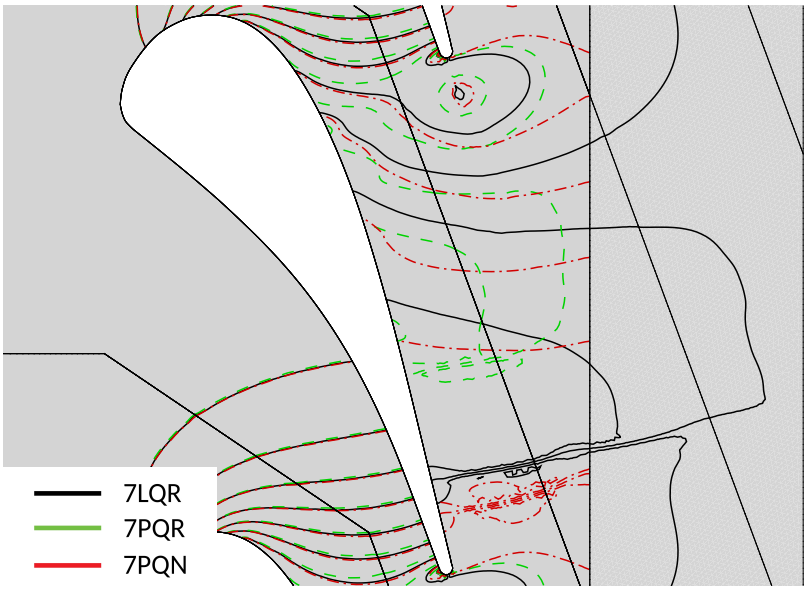

Figure 5: **MUR47 pressure fields comparison**

Results: MUR47 Figure 5 reports a comparison between the 7LQR, the 7PQR and the 7PQN static pressure fields. The solutions are similar only near the blade leading edge. Moving downstream, the 7PQR solution rapidly moves away from the 7LQR solution. In particular, in 7PQR the shock is positioned too early on the suction side (approximately $0.33c_{ax}$ before the trailing edge). Also the 7LQR and the 7PQN distributions are not superimposed, but the position of the shock in 7PQN (approximately $0.1c_{ax}$ before the trailing edge) is closer to the 7LQR case (approximately $0.15c_{ax}$ before the trailing edge).

The isentropic Mach number trends of 7LQR, 7PQR, 7PQN and 7PQE in the pitchwise direction at the probe outlet section are compared in Figure 6. The experimental data are also included. The shock is clearly visible in 7LQR and 7PQN and the position is almost the same, even though the shock magnitude seems to be higher in the 7PQN case. The 7LQR pressure is almost uniform along the pitch, as expected. In this case all the numerical data (not considering 7PQE) better fit the experiments, but they clearly predict a higher pressure variation. In fact, the experimental data show a smoother pitchwise variation of isentropic Mach number, thus suggesting that the shock intensity could be lower than the one obtained numerically. As expected, in the case of 7PQE the experimental profile is correctly reproduced. The bad accordance on the second pitch is to be ascribed to the non perfect periodicity of the experimental data.

The numerical isentropic Mach number distribution on the blade surface is compared to the known experimental values in Figure 7. The CFD results are in good accordance with each other only on the blade pressure side. Significant differences arise on the rear suction side, especially in terms of shock position. As observed before, compared to 7LQR, 7PQR locates the shock farther from the trailing edge, while 7PQN put it closer to the trailing edge. However, 7LQR is closer to 7PQN and they both better fit the experimental data. The 7PQE profile locates the shock better than the other cases but underestimates its intensity. The experimental shock position cannot be determined clearly looking at the suction side data, since the experimental isentropic Mach number smoothly moves from supersonic to subsonic between $0.8c_{ax}$ and $1.0c_{ax}$. The aerodynamic behaviour could be governed by the unsteady fluctuation of the

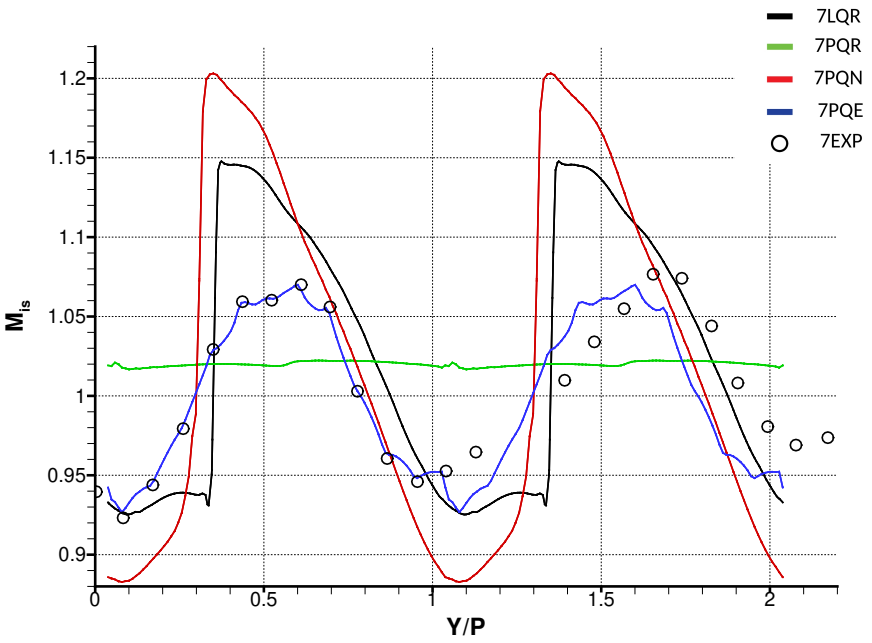

Figure 6: **MUR47 outlet isentropic Mach number distributions**

shock and this would justify the behaviour of the experimental data at the probes' location. Such unsteadiness cannot be reproduced by a purely steady calculation.

To better evaluate the performance of the NRBC-LEE method, the Schlieren visualisations are compared in Figure 8. Numerical Schlieren is calculated as the ratio between the density gradient magnitude and the local density value. All the numerical data are shown using the same variable range. As already observed, in the 7PQE case the shock is almost correctly positioned and its intensity is lower than in the other cases. It is interesting to observe that in the 7PQR case the shock is truncated near the wake region due to the constant pressure condition imposed at the probes' location. In the 7PQN case, the NRBC-LEE method allows for the extension of the shock up to the outlet section of the control volume, which is a more realistic behaviour. This is demonstrated by the experimental visualisation and by the 7PQE solution.

Results: loss coefficient Table 3 reports the area-averaged loss coefficients for all the investigated cases and for the experiments (EXP). The definition reported in Arts et al. (1990) is adopted for the calculation. The numerical values are not in accordance with the experimental ones, but this can be ascribed to the fact that a steady, fully turbulent calculation is performed. For the MUR43 case the numerical losses are almost doubled ($\approx +100\%$) with respect to the experimental value, while for the MUR47 case the difference is reduced ($\approx +50\%$). Furthermore, losses increase in the MUR47 case with respect to the MUR43 case due to the presence of the shock and this matches the experimental evidence. In the 7PQN case losses are higher than in the other cases, coherently with the increased shock intensity already observed in Figures from 6 to 8.

Results: exit angle Table 4 reports the area-averaged exit angle for all the numerical cases and for the experiments (EXP). In both MUR43 and MUR47 the exit flow angle is slightly

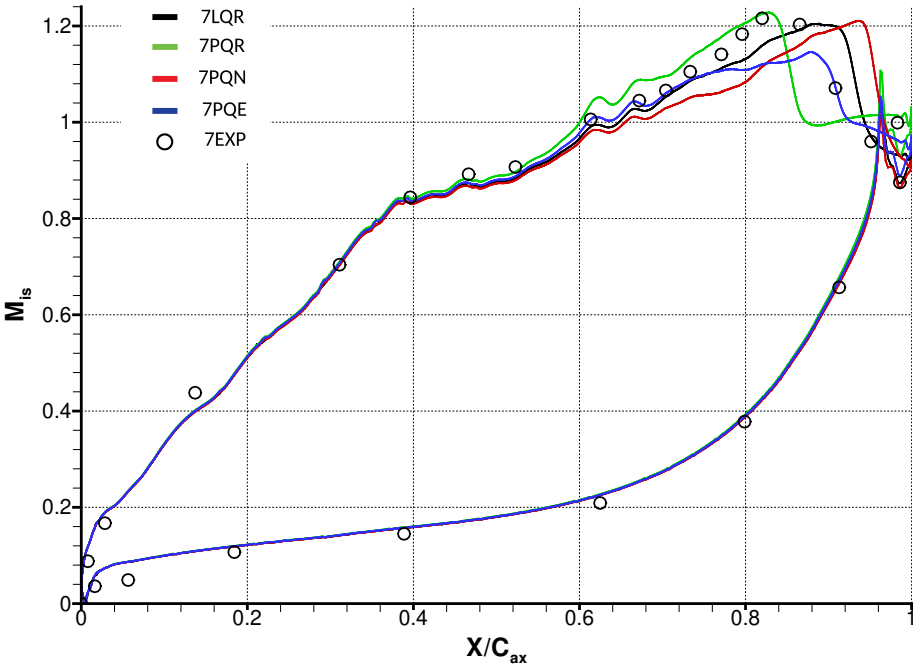

Figure 7: **MUR47 blade isentropic Mach number distributions**

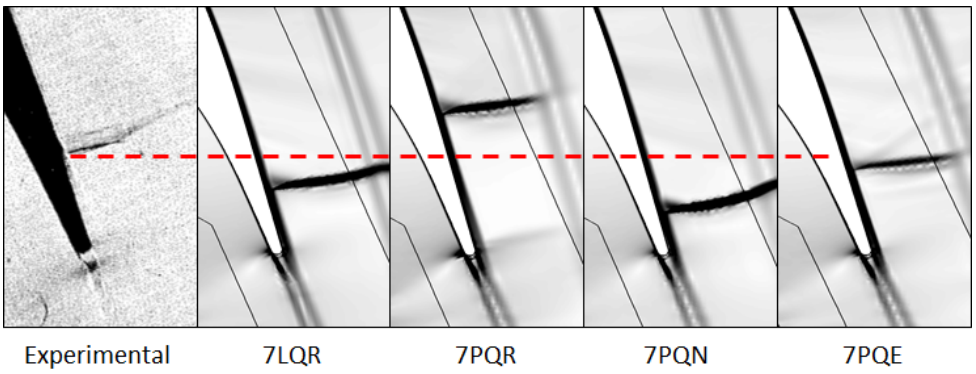

Figure 8: **MUR47 experimental (Arts et al. (1990)) and numerical Schlieren visualisation**

	LQR	**PQR**	**PQN**	**EXP**
MUR43	4.13%	4.33%	4.37%	2.19%
MUR47	4.73%	4.17%	5.39%	$\approx 3\%$

Table 3: **Area-averaged loss coefficients**

	LQR	PQR	PQN	EXP
MUR43	$74.74\,\mathrm{deg}$	$74.72\,\mathrm{deg}$	$74.84\,\mathrm{deg}$	$\approx 74.50\,\mathrm{deg}$
MUR47	$74.66\,\mathrm{deg}$	$74.78\,\mathrm{deg}$	$74.61\,\mathrm{deg}$	$\approx 74.15\,\mathrm{deg}$

Table 4: **Area-averaged exit angle**

($\approx 0.2\%$) overestimated by the CFD. In the MUR43 case 3PQR performs better than 3PQN in matching both the 3LQR and the experimental value. On the contrary, in the MUR47 case, 7PQN performs better than 7PQR in matching both the 7LQR and the experimental value. However, the effect of NRBC-LEE on the evaluation of the exit angle is very small and all the obtained values are very close to the experimental data.

CONCLUSIONS

A significant amount of research in CFD is dedicated to the development of increasingly accurate numerical tools. This target can be partially achieved by improving the numerical scheme used to solve the equations in the interior domain. However, the proper treatment of boundary conditions is still critical to achieve an effective increase in solver accuracy. The subject of absorbing boundary conditions is at least four decades old and a lot of proposals can be found in literature. The scientific results of the last fifteen years, are just a high-level refinement of the basic theories developed up to the 1990s.

This paper investigates the effects of the NRBC-LEE method, which is specifically focused on the simulation of turbomachinery flows. The results obtained after the implementation of the NRBC-LEE approach on the *HybFlow* solver demonstrate the importance of a correct treatment of the outlet boundary conditions for transonic flows. This implementation proves to be reliable for the reproduction of the pressure field of long domains on truncated domains. In fact, the flow field obtained on a truncated domain reproducing the LS89 test case shows mostly the same characteristics of the one obtained on a long domain. The impact of the NRBC-LEE approach on the evaluation of losses is also relevant, although shock losses tend to be overestimated. Finally, the use of NRBC-LEE method and the length of the domain seem to have limited impact on the mean exit flow angle, which is always close to the experimental value.

ACKNOWLEDGEMENTS

The authors want to thank sincerely Prof. Francesco Martelli (University of Florence), Prof. Marcello Manna (University of Naples "Federico II"), Prof. Mauro Carnevale (University of Bath) and Dr Nadia Loy (Polytechnic of Turin) for without them, this paper would not have been possible. The authors acknowledge the CINECA consortium for supporting this numerical activity in the frame of the ISCRA C-type IMPLICIT (Implementation and Testing of Navier-Stokes Characteristic Boundary Conditions in a Finite Volume Code for Turbomachinery Applications) project.

References

Abarbanel, S. & Gottlieb, D. (1997), 'A Mathematical Analysis of the PML Method', *Journal of Computational Physics* **134**(2), 357–363.

Anderson, W. K. & Bonhaus, D. L. (1994), 'An Implicit Upwind Algorithm for Computing Turbulent Flows on Unstructured Grids', *Computers and Fluids* **23**(1), 1–21.

Arts, T., Lambert de Rouvroit, M. & Rutherford, A. (1990), Aero-thermal investigation of a highly-loaded transonic linear turbine guide vane cascade, Technical report, Von Karman Institute for Fluid Dynamics.

Bayliss, A. & Turkel, E. (1982), 'Outflow Boundary Conditions for Fluid Dynamics', *SIAM Journal on Scientific and Statistical Computing* **3**(2), 250–259.

Berenger, J. P. (1994), 'A perfectly matched layer for the absorption of electromagnetic waves', *Journal of Computational Physics* **114**(2), 185–200.

Cação Ferreira, T. S., Vasilakopoulos, N. & Arts, T. (2019), 'Investigation of thermal effect on bypass transition on a high-pressure turbine guide vane', *Journal of Turbomachinery* **141**(5), 051006–051006–9.

Carnevale, M., Montomoli, F., D'Ammaro, A., Salvadori, S. & Martelli, F. (2013), 'Uncertainty quantification: A stochastic method for heat transfer prediction using les', *Journal of Turbomachinery* **135**(5), 051021–051021–8.

De Raedt, F. (2015), Non-Reflecting Boundary Conditions for non-ideal compressible fluid flows, PhD thesis, TU Delft.

Engquist, B. & Majda, A. (1977), 'Absorbing Boundary Conditions for the Numerical Simulation of Waves', *Mathematics of Computation* **31**(139), 629–651.

Giles, M. (1988), Non-Reflecting Boundary Conditions for the Euler Equations, Technical report, MIT Dept. of Aero and Astro.

Giles, M. (1990), 'Nonreflecting boundary conditions for Euler equation calculations', *AIAA Journal* **28**(12), 2050–2058.

Giles, M. (1991), UNSFLO: A Numerical Method For The Calculation Of Unsteady Flow In Turbomachinery, Technical report, MIT Dept. of Aeronautics and Astronautics.

Givoli, D. & Cohen, D. (1995), 'Nonreflecting boundary conditions based on Kirchhoff-type formulae', *Journal of Computational Physics* **117**(1), 102–113.

Givoli, D. & Neta, B. (2003), 'High-order non-reflecting boundary scheme for time-dependent waves', *Journal of Computational Physics* **186**(1), 24–26.

Gustafsson, B. (1988), 'Far-Field Boundary Conditions for Time-Dependent Hyperbolic Systems', *SIAM Journal on Scientific and Statistical Computing* **9**(5), 812–828.

Halpern, L. (1991), 'Artificial Boundary Conditions for Incompletely Parabolic Perturbations of Hyperbolic Systems', *SIAM Journal on Mathematical Analysis* **22**(5), 1256–1283.

Hedstrom, G. W. (1979), 'Nonreflecting boundary conditions for nonlinear hyperbolic systems', *Journal of Computational Physics* **30**(2), 222–237.

Hu, F. Q. (1996), 'On absorbing boundary conditions for linearized euler equations by a perfectly matched layer', *Journal of Computational Physics* **129**(1), 201–219.

Hu, F. Q. (2007), Boundary conditions: Acoustics, *in* 'Large-eddy simulation for acoustics, Wagner C., Huttl T., Sagaut P.', Cambridge University Press, pp. 216–220.

Montis, M., Ciorciari, R., Salvadori, S., Carnevale, M. & Niehuis, R. (2014), 'Numerical prediction of cooling losses in a high-pressure gas turbine airfoil', *Proceedings of the Institution of Mechanical Engineers, Part A: Journal of Power and Energy* **228**(8), 903–923.

Montomoli, F., Massini, M., Salvadori, S. & Martelli, F. (2011), 'Geometrical uncertainty and film cooling: Fillet radii', *Journal of Turbomachinery* **134**(1), 011019–011019–8.

Poinsot, T. J. & Lele, S. K. (1992), 'Boundary conditions for direct simulations of compressible viscous flows', *Journal of Computational Physics* **101**(1), 104–129.

Rudy, D. H. & Strikwerda, J. C. (1981), 'Boundary conditions for subsonic compressible Navier-Stokes calculations', *Computers and Fluids* **9**(3), 327–338.

Saad, Y. & Schultz, M. H. (1986), 'GMRES: A Generalized Minimal Residual Algorithm for Solving Nonsymmetric Linear Systems', *SIAM Journal on Scientific and Statistical Computing* **7**(3), 856–869.

Salvadori, S., Montomoli, F. & Martelli, F. (2013), 'Film-cooling performance in supersonic flows: effect of shock impingement', *Proceedings of the Institution of Mechanical Engineers, Part A: Journal of Power and Energy* **227**(3), 295–305.

Salvadori, S., Montomoli, F., Martelli, F., Adami, P., Chana, K. S. & Castillon, L. (2011), 'Aerothermal study of the unsteady flow field in a transonic gas turbine with inlet temperature distortions', *Journal of Turbomachinery* **133**(3), 031030–031030–13.

Saxer, A. P. & Giles, M. B. (1993), 'Quasi-three-dimensional nonreflecting boundary conditions for Euler equations calculations', *Journal of Propulsion and Power* **9**(2), 263–271.

Seguí, L. M., Gicquel, L. Y. M., Duchaine, F. & de Laborderie, J. (2018), 'Importance of boundary layer transition in a high-pressure turbine cascade using les'.

Thompson, K. W. (1990), 'Time-dependent boundary conditions for hyperbolic systems, II', *Journal of Computational Physics* **89**(2), 439–461.

Tsynkov, S. V. (1998), 'Numerical solution of problems on unbounded domains. A review', *Applied Numerical Mathematics* **27**(4), 465–532.

Wilcox, D. C. (1993), 'Turbulence modeling for CFD', *La Canada, CA: DCW industries* pp. 84–87.